International Journal of Heat and Mass Transfer 116 (2018) 969–976

Contents lists available at ScienceDirect

International Journal of Heat and Mass Transfer

journal homepage: www.elsevier.com/locate/ijhmt

# Lattice Boltzmann simulation of shear viscosity of suspensions containing porous particles

A. Xu, L. Shi, T.S. Zhao *

*HKUST Energy Institute, Department of Mechanical and Aerospace Engineering, The Hong Kong University of Science and Technology, Hong Kong, China*

ARTICLE INFO

*Article history:*
Received 1 July 2017
Received in revised form 11 September 2017
Accepted 17 September 2017
Available online 28 September 2017

*Keywords:*
Relative viscosity
Porous particle
Particle flow
Lattice Boltzmann method

ABSTRACT

We present three-dimensional lattice Boltzmann simulations of dilute suspensions containing porous particles. The fluid flow around and inside a porous particle is described by the volume-averaged macroscopic equations in terms of intrinsic phase average. The energy dissipation of the suspended particle in a Couette flow is calculated to obtain the relative viscosity of the suspension. Results show that the relative viscosity of the suspension increases linearly with the particle volume fraction. A correlation equation is obtained for the intrinsic viscosity as a function of Darcy number. It is found that when the suspension is at the inertial flow regime, its intrinsic viscosity increases linearly with Reynolds number, and the increasing rate depends on Darcy number.



## 1. Introduction

Suspended solid particles in a fluid are ubiquitous in nature and have wide applications in industry. Determining the rheology of a particle suspension is important to control industrial flow processes accurately [1]. The rheology of a suspension is usually characterized by the relative viscosity $\eta_r$, which is the ratio between effective viscosity of a suspension and viscosity of the base fluid. The first theoretical study to determine the relative viscosity may date back to 1906, when Einstein derived the mathematical expression $\eta_r = 1 + \langle\bar{\eta}\rangle\phi$ for a dilute suspension containing spherical particles [2]. Here, $\phi$ is solid particle volume fraction, $\langle\bar{\eta}\rangle$ is intrinsic viscosity and takes the value of $\langle\bar{\eta}\rangle = 2.5$. Afterwards, to study a semi-dilute suspension that has higher particle volume fraction, the relationship $\eta_r = 1 + \langle\bar{\eta}\rangle\phi + \langle\bar{\eta}\rangle_1\phi^2 + \cdots$ was proposed in which higher order terms of $\phi$ were included [3]. For a concentrated suspension that has even higher particle volume fraction of $\phi > 25\%$, the relationship $\eta_r = (1 - \phi/\phi_m)^{-B\phi_m}$ was proposed so that the relative viscosity would approach infinite when the particle volume fraction is approaching the densest possible packing fraction $\phi_m$ [4]. In addition to suspensions of spherical particles, research attentions are also drawn on non-spherical particles. Examples include Jeffery's analytical solution of relative viscosity for suspensions of ellipsoidal particles that are prolate or oblate [5]. Recently, with the tremendous increase in computational capability, first-principle-based modeling techniques that are capable of handling complex moving boundary problems are also adopted as an alternative strategy to determine the rheology of suspensions [6–11]. The basic idea behind these numerical approaches is to obtain the energy dissipation of the suspended particle in a Couette flow through direct numerical simulation of the flow field. For example, Lishchuk et al. [7] calculated the shear viscosity of suspensions of spherical particles and reproduced both the Einstein's relation for low particle volume fraction and Krieger-Dougherty's relation for high particle volume fraction. Moreover, these numerical approaches do not restrict the flow at low Reynolds number ($Re$), which allows to investigate the dependence of intrinsic viscosity on $Re$. For example, Kulkarni and Morris [8] reported the relative viscosity of suspension of spherical particles at $0.01 \leqslant Re < 5$. They showed that inertia can increase the particle contribution to the effective viscosity of the suspension. Huang et al. [11] found that for dilute prolate and oblate spheroidal suspensions, the intrinsic viscosity changes linearly with $Re$ at low-$Re$ regime and nonlinearly at high-$Re$ regime.

The above studies focused on solid particles that are impermeable to fluid, while in real-world applications, porous particles that are permeable to fluids are also frequently encountered, such as core-shell like particles, catalyst clusters, encapsulated drugs, and so on [12–14]. Efforts have been devoted to study the effect of permeability of the porous particle on the flow pattern and the particle-fluid interactions [15,16]. For example, Masoud et al. [15] theoretically investigated the dynamics of porous elliptical particle in shear flow. They concluded that although the flow field inside and around the particle significantly depends on the permeability of the porous particle, the permeability has little effect on

* Corresponding author.
*E-mail address:* metzhao@ust.hk (T.S. Zhao).

https://doi.org/10.1016/j.ijheatmasstransfer.2017.09.060
0017-9310/

the rotational behavior of the porous particle. Later, Li et al. [16] numerically investigated the dynamics of porous circular particle in shear flow. They found Masoud et al.'s conclusion is only validated when the fluid inertia is negligible or the confinement effect of the bounding walls is weak.

Although progress has been made on the research of suspensions containing porous particles, to the best of our knowledge, there is no investigation on its rheology with the aid of first-principle-based modeling techniques. In this work, we present three-dimensional lattice Boltzmann (LB) simulation of a dilute suspension containing porous particle to determine the relative viscosity. To describe the fluid flow around and inside a porous particle, the general volume-averaged conservation equations are adopted [16–18]. When the fluid motion is sufficient slow, the Darcy's law [19] and the Brinkman-Debye-Bueche (BDB) equation [20,21] can be recovered; when the flow Reynolds number is finite, the inertial effect on the flow inside and around the porous particle can be incorporated. More importantly, the continuity of both fluid velocity and shear stress at the interface between the porous region and the free flow is ensured through the incorporating of a second-order viscous term in the volume-averaged macroscopic governing equation. Here, the lattice Boltzmann (LB) method is chosen to obtain the numerical solution due to its simplicity, accuracy, and parallelism for simulating complex multiphase flows [22–24].

## 2. Numerical method

### 2.1. Volume-averaged macroscopic governing equations

The fluid flow around and inside the porous particle is described by the volume-averaged equations in terms of intrinsic phase average proposed by Wang et al. [18], which is written as

$$\nabla \cdot \langle \mathbf{u}_f \rangle^f = 0 \tag{1}$$

$$\frac{\partial \langle \mathbf{u}_f \rangle^f}{\partial t} + \langle \mathbf{u}_f \rangle^f \cdot \nabla \langle \mathbf{u}_f \rangle^f = -\frac{1}{\rho_f} \nabla \langle p_f \rangle^f + \nu \nabla^2 \langle \mathbf{u}_f \rangle^f + \mathbf{F}_m \tag{2}$$

where $\rho_f$ is the fluid density and $\nu$ is the fluid viscosity. $\mathbf{u}_f$ and $p_f$ are the local fluid velocity and pressure, respectively. Here, the intrinsic phase average is defined as $\langle \psi_k \rangle^k = \frac{1}{V_k} \int_{V_k} \psi_k dV$, and the phase average is defined as $\langle \psi_k \rangle = \frac{1}{V} \int_{V_k} \psi_k dV$. $V_k$ denotes the volume of the $k$-phase within the representative volume $V$. $\psi_k$ is a quantity associated with the $k$-phase. The subscript $s$ and $f$ represent solid and fluid phase, respectively. The total body force $\mathbf{F}_m$ in Eq. (2) is given by [18]

$$\mathbf{F}_m = -\frac{\varepsilon \nu}{K} \left( \langle \mathbf{u}_f \rangle^f - \langle \mathbf{u}_s \rangle^s \right) - \frac{\varepsilon^2 F_\varepsilon}{\sqrt{K}} \left( \langle \mathbf{u}_f \rangle^f - \langle \mathbf{u}_s \rangle^s \right) \left| \langle \mathbf{u}_f \rangle^f - \langle \mathbf{u}_s \rangle^s \right| \tag{3}$$

where $\varepsilon$ is the porosity of the porous particle. The first and the second terms on the right-hand side of Eq. (3) are the linear Darcy drag and nonlinear Forchheimer drag due to the existence of porous medium, respectively. Because the porous particle moves as a rigid-body, its translational and rotational velocities does not change after taking the intrinsic phase averaging. Then, the intrinsic phase-average velocity of the solid particle $\langle \mathbf{u}_s \rangle^s$ is calculated as $\langle \mathbf{u}_s \rangle^s = \mathbf{u}_s$. The permeability $K$ quantifies the ability of the porous particle to transmit fluids. $F_\varepsilon$ is the geometric function and it is given as $F_\varepsilon = 1.75/\sqrt{150\varepsilon^3}$ following Ergun's correlation. The porous structure inside the particle is described by the permeability $K$ and the porosity $\varepsilon$, which can be correlated via the relation $K = \varepsilon^3 d_p^2 / \left[ 150(1-\varepsilon)^2 \right]$ to simplify the problem. Here, $d_p$ is the characteristic diameter of filling grains within the porous particle. In the limit of $\varepsilon \to 0$, the porous particle would reduce to an impermeable particle; while in the limit of $\varepsilon \to 1$, the regime occupied by the porous particle would be filled with fluid. The dimensionless numbers characterize the system are the particle Reynolds number ($Re_p$) and Darcy number ($Da$), which are defined as

$$Re_p = \frac{\Gamma D^2}{\nu}, \quad Da = \frac{K}{D^2} \tag{4}$$

where $\Gamma$ is the shear rate, and $D$ is the diameter of the porous particle.

### 2.2. Lattice Boltzmann model for volume-averaged equations

In LB method, to solve Eqs. (1) and (2), the evolution equation of density distribution function can be written as

$$f_i(\mathbf{x} + \mathbf{e}_i \delta_t, t + \delta_t) - f_i(\mathbf{x}, t) = -\left[ f_i(\mathbf{x}, t) - f_i^{(\mathrm{eq})}(\mathbf{x}, t) \right] + \delta_t F_i, \quad (i = 0, 1, \ldots, 18) \tag{5}$$

where $f_i$ is the density distribution function, $t$ is the time, $\delta_t$ is the time step, $\mathbf{x}$ is the fluid parcel position. $\mathbf{e}_i$ is the discrete velocity along the $i$th direction, and is given as

$$[\mathbf{e}_0, \mathbf{e}_1, \mathbf{e}_2, \mathbf{e}_3, \mathbf{e}_4, \mathbf{e}_5, \mathbf{e}_6, \mathbf{e}_7, \mathbf{e}_8, \mathbf{e}_9, \mathbf{e}_{10}, \mathbf{e}_{11}, \mathbf{e}_{12}, \mathbf{e}_{13}, \mathbf{e}_{14}, \mathbf{e}_{15}, \mathbf{e}_{16}, \mathbf{e}_{17}, \mathbf{e}_{18}] = c \begin{bmatrix} 0 & 1 & -1 & 0 & 0 & 0 & 0 & 1 & -1 & 1 & -1 & 1 & -1 & 1 & -1 & 0 & 0 & 0 & 0 \\ 0 & 0 & 0 & 1 & -1 & 0 & 0 & 1 & 1 & -1 & -1 & 0 & 0 & 0 & 0 & 1 & -1 & 1 & -1 \\ 0 & 0 & 0 & 0 & 0 & 1 & -1 & 0 & 0 & 0 & 0 & 1 & 1 & -1 & -1 & 1 & 1 & -1 & -1 \end{bmatrix} \tag{6}$$

where $c = \delta_x / \delta_t$ is lattice constant, and $c = \delta_x = \delta_t = 1$ is adopted in this work. The equilibrium particle distribution function is

$$f_i^{(\mathrm{eq})}(\mathbf{x}, t) = \rho_f \omega_i \left[ 1 + \frac{\mathbf{e}_i \cdot \langle \mathbf{u}_f \rangle^f}{c_s^2} + \frac{\left( \mathbf{e}_i \cdot \langle \mathbf{u}_f \rangle^f \right)^2}{2c_s^4} - \frac{|\langle \mathbf{u}_f \rangle^f|^2}{2c_s^2} \right], \quad (i = 0, 1, \ldots, 18) \tag{7}$$

where the weights are $\omega_0 = 1/3$, $\omega_{1-6} = 1/18$, $\omega_{7-18} = 1/36$, and $c_s^2 = 1/3c^2$ is the lattice sound speed. The forcing term is given by [16]

$$F_i = \rho_f \omega_i \left( 1 - \frac{1}{2\tau} \right) \left[ \frac{\mathbf{e}_i \cdot \mathbf{F}_m}{c_s^2} + \frac{\mathbf{e}_i \cdot \langle \mathbf{u}_f \rangle^f}{c_s^4} (\mathbf{e}_i \cdot \mathbf{F}_m) - \frac{\langle \mathbf{u}_f \rangle^f \cdot \mathbf{F}_m}{c_s^2} \right], \quad (i = 0, 1, \ldots, 18) \tag{8}$$

The macroscopic density $\rho$ is calculated as

$$\rho = \sum_{i=0}^{18} f_i \tag{9}$$

The macroscopic velocity $\langle \mathbf{u}_f \rangle^f$ is calculated as

$$\langle \mathbf{u}_f \rangle^f = \frac{\mathbf{v}}{d_0 + \sqrt{d_0^2 + d_1|\mathbf{v}|}} + \langle \mathbf{u}_s \rangle^s, \quad \rho \mathbf{v} = \sum_{i=0}^{18} \mathbf{e}_i f_i - \rho_f \langle \mathbf{u}_s \rangle^s \tag{10}$$

where $\mathbf{v}$ is the temporal variable. Two parameters $d_0$ and $d_1$ are given as

$$d_0 = \frac{1}{2}\left(1 + \frac{\delta_t}{2}\frac{\varepsilon \nu}{K}\right), \quad d_1 = \frac{\delta_t}{2}\frac{\varepsilon^2 F_\varepsilon}{\sqrt{K}} \tag{11}$$

### 2.3. Particle-resolved method for suspension

The translational and rotational motion of the particles are determined by Newton's second law and Euler's second law, respectively

$$M_p \frac{d\mathbf{U}(t)}{dt} = \mathbf{F}(t) \tag{12}$$

$$\mathbf{I}_p \cdot \frac{d\boldsymbol{\Omega}(t)}{dt} + \boldsymbol{\Omega}(t) \times \left[\mathbf{I}_p \cdot \boldsymbol{\Omega}(t)\right] = \mathbf{T}(t) \tag{13}$$

where $M_p$ is the mass of the particle, and $\mathbf{I}_p$ is the inertial tensor of the particle. To calculate the force and torque exerted on the particle by the fluid, the momentum-exchange method is adopted due to its simplicity and robustness [25,26]. Specifically, the modified form proposed by Wen et al. [27] is considered in this work to calculate the total force $\mathbf{F}$ and torque $\mathbf{T}$ as

$$\mathbf{F} = \sum_{\mathbf{x}_f} \sum_{i_{bl}} \left[f_i^+(\mathbf{x}_f, t)(\mathbf{e}_i - \mathbf{u}_w) - f_{\bar{i}}(\mathbf{x}_f, t + \delta_t)(\mathbf{e}_{\bar{i}} - \mathbf{u}_w)\right] \tag{14}$$

$$\mathbf{T} = \sum_{\mathbf{x}_f} \sum_{i_{bl}} (\mathbf{x}_w - \mathbf{x}_c) \times \left[f_i^+(\mathbf{x}_f, t)(\mathbf{e}_i - \mathbf{u}_w) - f_{\bar{i}}(\mathbf{x}_f, t + \delta_t)(\mathbf{e}_{\bar{i}} - \mathbf{u}_w)\right] \tag{15}$$

where $\mathbf{x}_f$ is the fluid node and $\mathbf{u}_w$ is the velocity of the moving particle surface. $f_i^+$ denotes the post-collision distribution function, and $f_i$ denotes the distribution function associated with the velocity $\mathbf{e}_{\bar{i}} = -\mathbf{e}_i$. It should be noted that at the particle's surface, no special treatment (such as interpolation of density distribution function) is required as opposed to that for impermeable particles [26,28]. This is because a second-order viscous term is already included in the volume-averaged macroscopic governing equations to ensure the continuity of both fluid velocity and shear stress at the interface.

### 2.4. Calculating relative viscosity

For a neutrally buoyant particle in Couette flow, the relative viscosity of the suspension is calculated as

$$\eta_r = \frac{\eta_s}{\eta_{bf}} = \frac{\langle \sigma \rangle / \Gamma}{\rho \nu} \tag{16}$$

where $\eta_s$ and $\eta_{bf}$ are effective viscosity of the suspension and viscosity of the base fluid, respectively. In the simulations, the porous particle is placed in the center of the simulation box as illustrated in Fig. 1. The upper and lower walls move with speed $U$ in opposite directions. The velocity boundary condition is applied at these boundaries, and the modified half-way bounce-back scheme proposed by Ladd [29,30] is adopted to determine the distribution function at the first and last layer of fluid nodes in the computational domain, which is written as $f_{\bar{i}}(\mathbf{x}_f, t + \delta_t) = f_i^+(\mathbf{x}_f, t) - 2\omega_i \rho(\mathbf{x}_f) \frac{\mathbf{e}_i \cdot \mathbf{u}_w}{c_s^2}$. Here, $\mathbf{u}_w$ is the velocity of the moving wall. The distance between the two moving walls is $L = N_z$, thus the shear rate of the Couette flow is $\Gamma = 2U/N_z$. Following Huang et al.'s work [9], the average shear stress $\langle \sigma \rangle$ can be obtained through averaging the shear stress acting on the moving flat wall over time. Here, the streamlines of the Couette flow are in $x$ direction and the velocity gradient is in $z$ direction, the shear stress at a fluid node is calculated as $\sigma = \rho \nu (\partial_z u + \partial_x w) = -(1 - \frac{1}{2\tau}) \sum_{i=0}^{18} \left(f_i - f_i^{(\mathrm{eq})}\right) \mathbf{e}_{ix} \mathbf{e}_{iz}$ using LB method, where $u$ and $w$ are the components of velocity vector $\mathbf{u}$ in $x$ and $z$ directions, respectively.

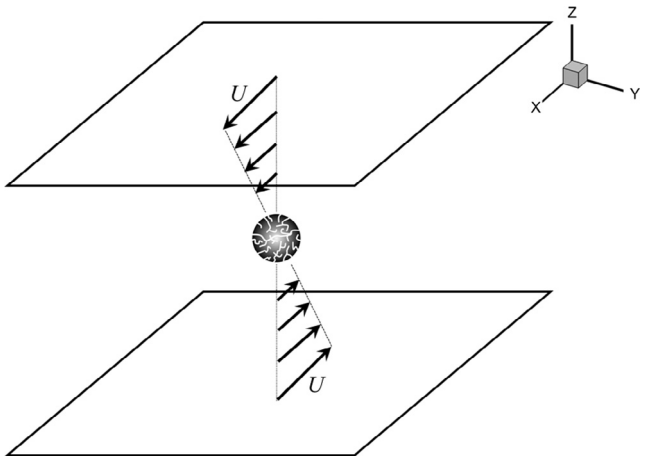


**Fig. 1.** Schematic drawing of the simulation settings.

## 3. Results and discussion

### 3.1. Validation I: Torque on the porous particle

We consider the three-dimensional problem of torque exerted on a porous sphere. Previous analytical studies shown that at the creeping flow regime, a porous sphere in a simple shear flow of strength $\Gamma$ experienced the same torque as the porous sphere rotating with an angular velocity $\Omega = \Gamma/2$ in a quiescent fluid [15,31]. Specifically, the torque is [31]

$$\mathbf{T}_y = -\pi \mu \omega_y D^3 \left(\frac{\beta^2 + 3 - 3\beta \coth \beta}{\beta^2}\right) \mathbf{e}_y \tag{17}$$

where $\beta = 1/(2\sqrt{Da})$. Here, the component of the particle's angular velocity $\omega_y = \Omega = \Gamma/2$.

In the simulations, three mesh sizes $N_x \times N_y \times N_z = 80 \times 80 \times 80$, $120 \times 120 \times 120$ and $160 \times 160 \times 160$ are adopted. The diameter of the porous particle ($D$) is chosen so that the confinement ratio is $N_z/D = 4$. The density of the fluid and the density of the particle are set the same, namely a neutrally buoyant porous sphere is considered. Periodical boundary conditions are applied in the $x$ and $y$ directions. For the case of the porous sphere in a simple shear flow, the upper and lower walls move in opposite direction with the same speed $U = \Gamma N_z/2$; for the case of the porous sphere rotating with an angular velocity, the upper and lower walls are set as stationary. The particle Reynolds number is set as $Re_p = 0.01$ to ensure the system is at the creeping flow regime; the Darcy number is chosen between $10^{-1}$ and $10^{-6}$. From Fig. 2, we can see that the simulation results agree with the analytical results in both the scenarios. Moreover, the results demonstrate the grid convergence of the numerical method, the confinement ratio of $N_z/D = 4$ is adequate to minimize the boundary effect, and 30 grids are adequate to resolve the diameter of the porous spherical particle. In the following, unless otherwise mentioned, the computational mesh size is chosen as $N_x \times N_y \times N_z = 160 \times 160 \times 160$ and the diameter of the particle is chosen between 30 and 40 lattice.

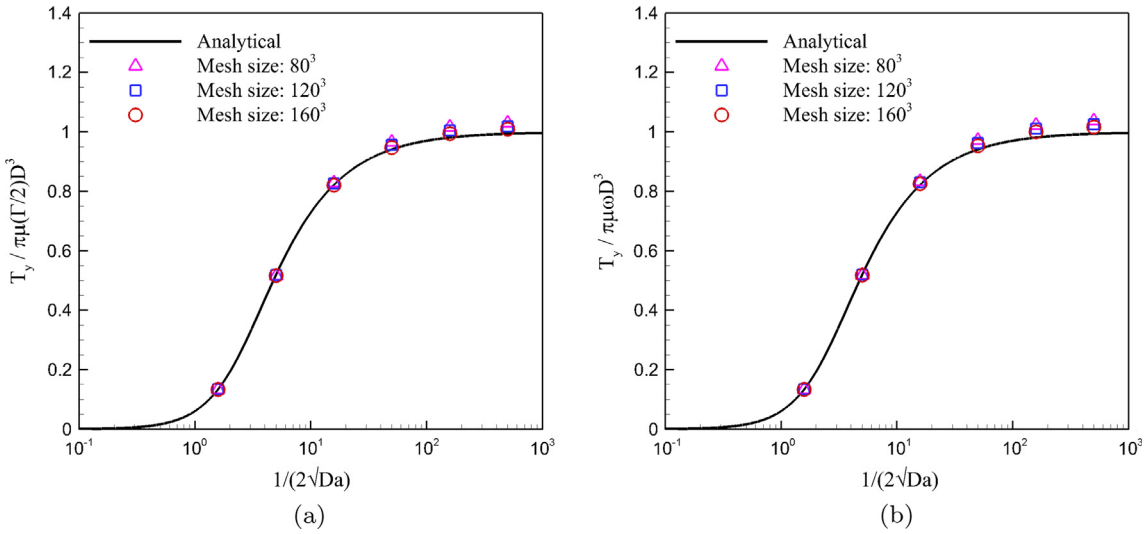


**Fig. 2.** Dimensionless torque as a function of the dimensionless permeability. (a) The particle is stationary in a simple shear flow; (b) the particle rotates in quiescent fluid.

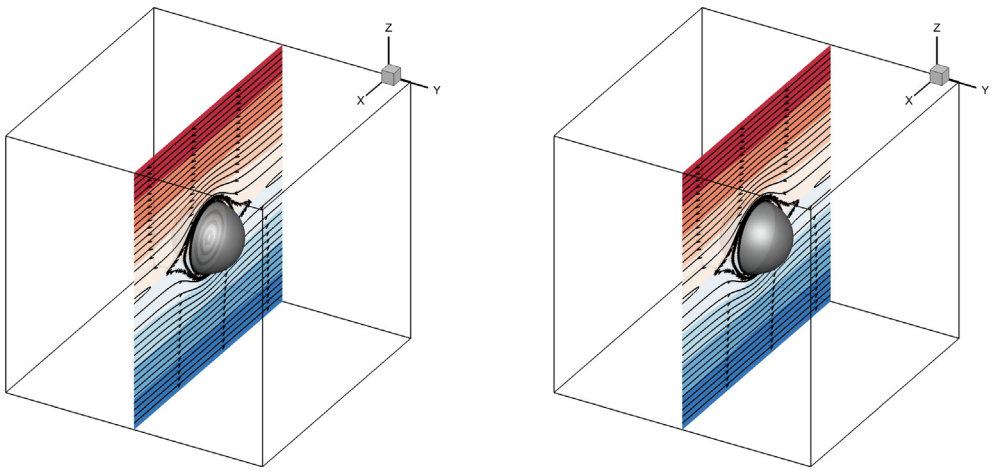


**Fig. 3.** Streamlines for a freely rotating spherical particle in a simple shear flow ($Re_p = 0.01$), the slice shows the velocity of the fluid in horizontal direction.

### 3.2. Validation II: Relative viscosity of a suspension of impermeable particle

In the limit of $Da \to 0$, the porous particle would reduce to an impermeable solid particle. Fig. 3(a) shows the streamlines for a freely rotating porous spherical particle in a simple shear flow at $Da = 10^{-6}$. A small particle Reynolds number $Re_p = 0.01$ is chosen. The diameter of the porous particle is $D = 40$ lattice. We can see that at this sufficiently small Darcy number, there is indeed no streamlines penetrating the particle. In comparison, Fig. 3(b) shows the streamlines for a freely rotating impermeable spherical particle under the same scenario. The flow field around the impermeable particle is very similar with that for the porous particle with $Da = 10^{-6}$. For interested readers, the implementation details of simulating the motion of impermeable rigid particles in a viscous fluid can be found in Ref. [28,32].

For the dilute suspensions of solid spherical particles that are impermeable, the relative viscosity is given as $\eta_r = 1 + 2.5\phi$ following Einstein's relation, as illustrated by the solid black line in Fig. 4. The red[1] circles in Fig. 4 represent the relative viscosity of the suspension of porous spherical particle at $Da = 10^{-6}$. In the simulations, the mesh size is $160 \times 160 \times 160$, the diameter of the porous particle is varied between 30 and 40 lattice to adjust the particle volume fraction, thus, the confinement ratio is $N_z/D \geqslant 4$ which can avoid moving wall effect. Accordingly, the particle volume fraction is below 1% and the suspension can be regarded as a dilute suspension. To further decrease the confinement ratio so that suspension with larger particle volume fraction can be simulated, the Lees-Edwards boundary condition [33,34] may be adopted in future study. A linear fit of the data (illustrated by the blue dash line) in Fig. 4 gives the slope equals to 2.5583 with coefficients of determination as 0.9999, which indicates that the relative error for the calculation of intrinsic viscosity is 2.3%.

[1] For interpretation of color in Figs. 4 and 9, the reader is referred to the web version of this article.

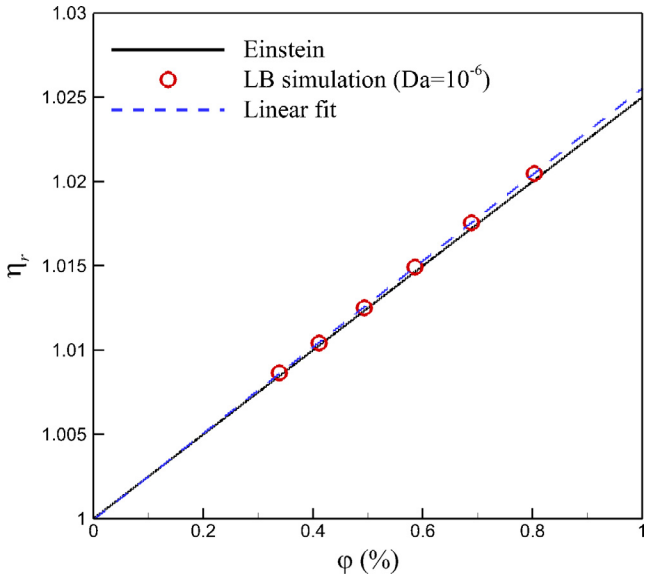


**Fig. 4.** Relative viscosity of the suspension as a function of particle volume fraction ($Re_p = 0.01$).

### 3.3. Relative viscosity of a dilute suspension of porous particle

We first consider the suspension of porous particle at small Reynolds number. The particle Reynolds number is chosen as $Re_p = 0.01$ so that the inertia of the particle and the fluids can be neglected. Fig. 5 shows the flow field inside and around the porous particle at $Da = 10^{-1}, 10^{-2}, 10^{-3}$, and $10^{-4}$. The results demonstrate that Darcy number has a strong influence on the flow pattern: the porous particle with larger Darcy number allows more streamlines to pass through, which is consistent with our intuition. At $Da = 10^{-1}$ as shown in Fig. 5(a), we can clearly observe the penetration of streamlines through the porous particle. On the other hand, at small Darcy number, e.g., $Da = 10^{-4}$ shown in Fig. 5(d), the streamlines within the porous particle are almost not affected by the flow field around the porous particle, and are merely the results of the particle's rotation. To quantitatively describe the effects of Darcy number on the flow pattern, we calculate the dimensionless flow rate through the porous particle as $Q_{\text{porous}}/Q_{\text{permeable}}$ and the dimensionless particle's rotational angular velocity as $\omega/\Gamma$, as shown in Fig. 6. Here, the flow rate $Q_{\text{porous}}$ is calculated as the average of velocity component $u$ through the $x$ half-plane and only the top-half cross-section area is considered due to the symmetry of the computational domain; $Q_{\text{permeable}}$ denotes the flow rate of the Couette flow through the same area. The general trend agrees with that of 2D porous particle in shear flow reported by Li et al. [16]. Fig. 7 further presents the pressure $\Delta p$ contours, where $\Delta p = (p - p_0)/(\rho_0 U^2/2)$ and $p_0 = c_s^2 \rho_0$. We can see that the torques produced by the shear stress are in opposite directions and are in balance at the steady state. It is also found that the pressure pattern is not affected by the Darcy number except its maximum and minimum intensities.

For the dilute suspension of porous spherical particle, the relative viscosity as a function of particle volume fraction at different Darcy numbers is shown in Fig. 8. Linear fits of the data give the coefficient of determination above 0.9999 in all the cases, indicating that the relative viscosity increases linearly with the particle volume fraction. Similar with the dilute suspension of impermeable spherical particles, here we propose that at small Reynolds number, the relative viscosity of a dilute suspension of porous spherical particles can be calculated as $\eta_r = 1 + \langle \bar{\eta}(Da) \rangle \phi$, where

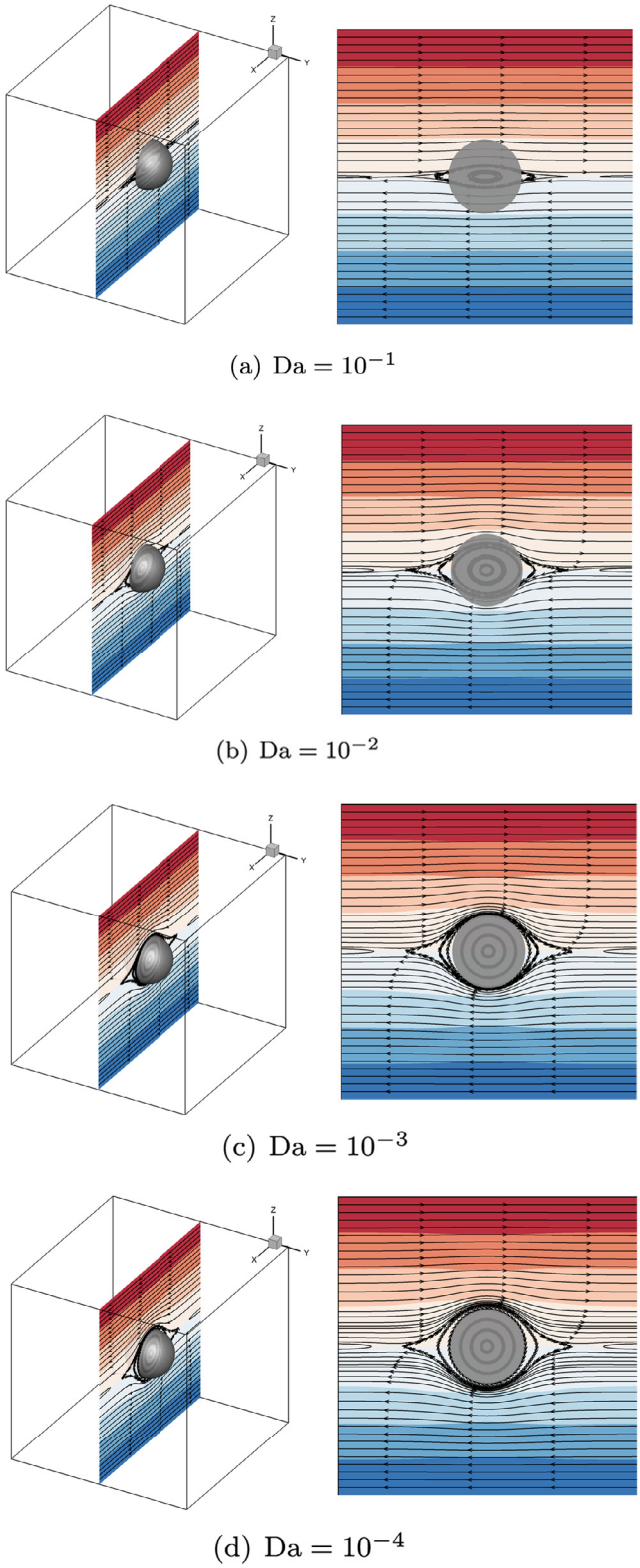


**Fig. 5.** Streamlines for a freely rotating porous spherical particle in simple shear flow ($Re_p = 0.01$), the slice shows the velocity of the fluid in horizontal direction.

$\langle \bar{\eta}(Da) \rangle$ is the intrinsic viscosity of the suspension depending on Darcy number.

We further discuss the intrinsic viscosity $\langle \bar{\eta}(Da) \rangle$. As shown in Fig. 9, the red circles represent the intrinsic viscosity of the suspension at different Darcy numbers; the red dash dot line represents

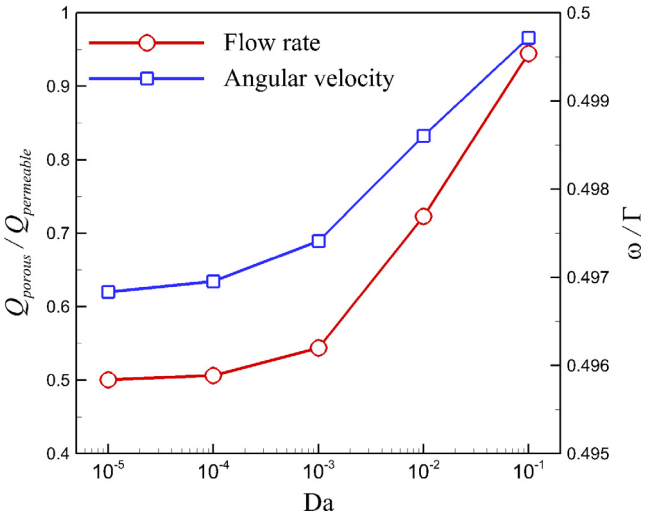


**Fig. 6.** Dimensionless flow rate and rotational angular velocity for a freely rotating porous spherical particle in simple shear flow ($Re_p = 0.01$).

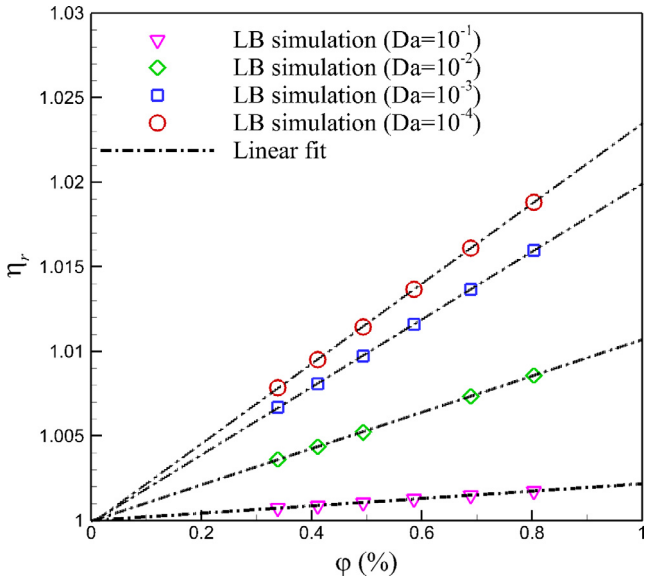


**Fig. 8.** Relative viscosity of the suspension of porous particle as a function of particle volume fraction ($Re_p = 0.01$).

the intrinsic viscosity given by Einstein's relation for suspension of impermeable spherical particles, which is the limit for $\langle\bar{\eta}(Da)\rangle$ when $Da \to 0$. The results show that there exists a critical Darcy number at $Da_c \approx 10^{-3}$ above which the relation between $\log(Da)$ and $\langle\bar{\eta}(Da)\rangle$ is linear, namely, $\langle\bar{\eta}(Da)\rangle = -0.9797\log(Da) - 0.8886$ for $10^{-3} \leqslant Da \leqslant 10^{-1}$. Below this critical Darcy number, the relation between $\log(Da)$ and $\langle\bar{\eta}(Da)\rangle$ can be described by a second-degree polynomial fit, namely, $\langle\bar{\eta}(Da)\rangle = -0.1321[\log(Da)]^2 -$

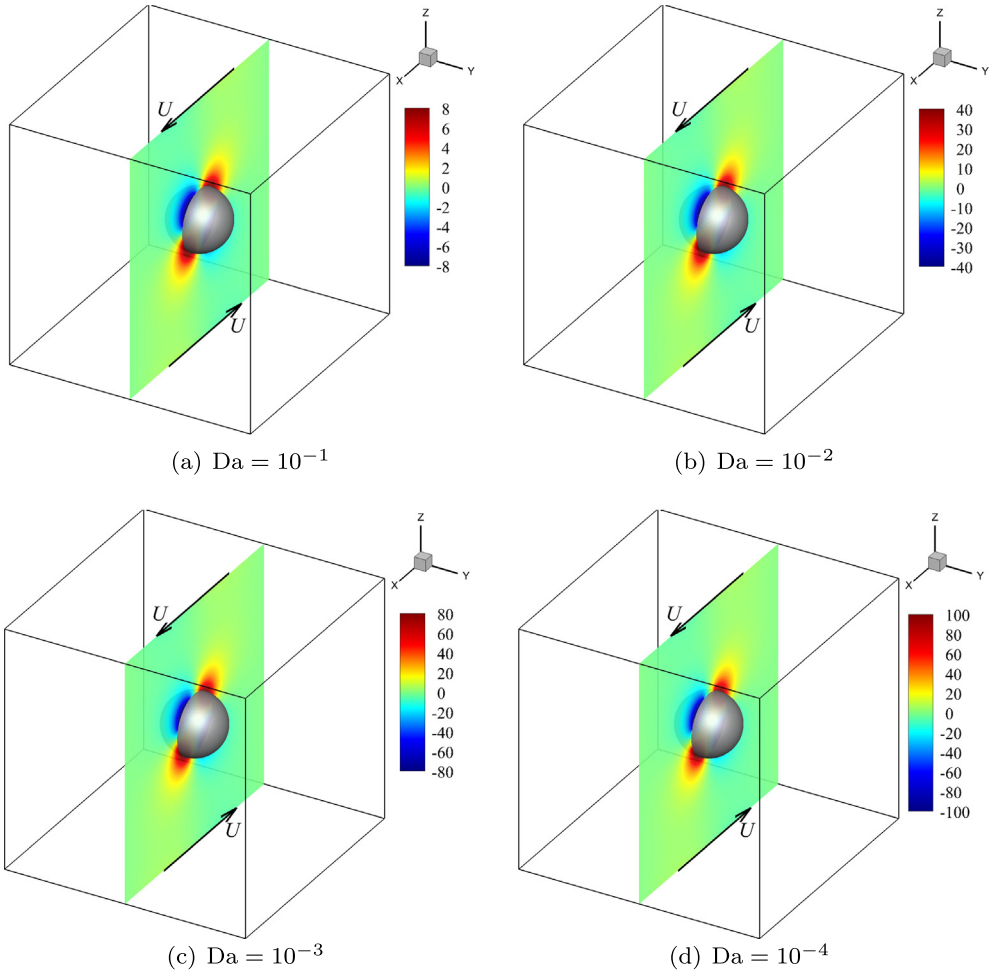


**Fig. 7.** Pressure $\Delta p$ contours for a freely rotating porous spherical particle in simple shear flow ($Re_p = 0.01$).

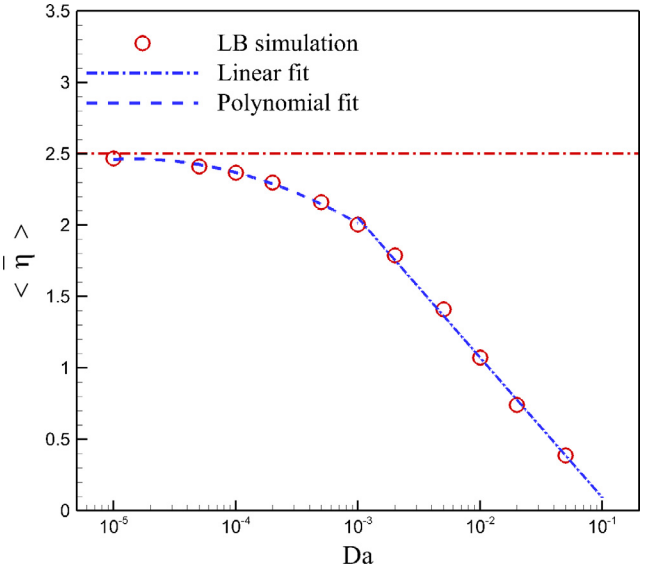


**Fig. 9.** Intrinsic viscosity of the suspension of porous particle at different Darcy numbers ($Re_p = 0.01$).

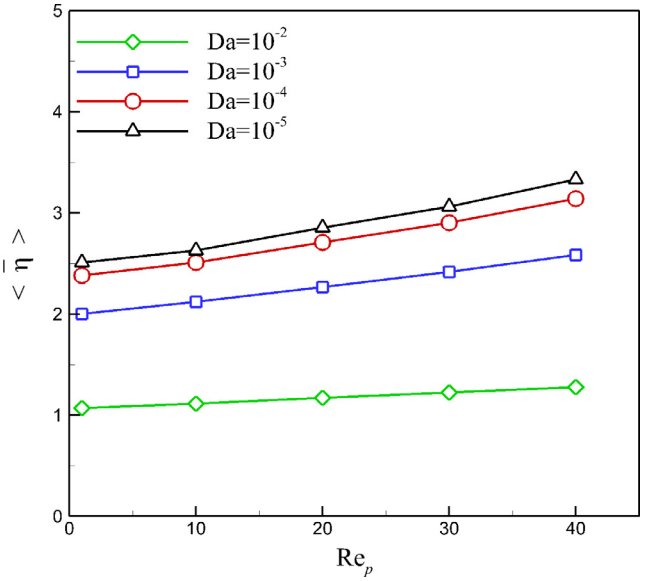


**Fig. 10.** Intrinsic viscosity of the suspension of porous particle as functions of Reynolds numbers.

**Table 1**
Linear fits of the $\langle \bar{\eta} \rangle - Re$ curve for dilute suspensions of porous spherical particles.

| $Da$ | $\langle \bar{\eta}_0 \rangle$ | $k$ | Coefficient of determination |
|---|---|---|---|
| $10^{-2}$ | 1.0636 | 0.0054 | 0.9993 |
| $10^{-3}$ | 1.9780 | 0.0149 | 0.9976 |
| $10^{-4}$ | 2.3343 | 0.0196 | 0.9911 |
| $10^{-5}$ | 2.4426 | 0.0213 | 0.9826 |

$1.2806\log(Da) - 0.6394$ for $10^{-5} \leqslant Da < 10^{-3}$. For both fits, the coefficients of determination is above 0.99, indicating the proposed scaling law is reliable.

We now consider the inertial effects on the intrinsic viscosity of a suspension of porous particles. Fig. 10 shows the intrinsic viscosity as a function of particle Reynolds number for the porous spherical particles at different Darcy numbers. The intrinsic viscosity $\langle \bar{\eta}(Da) \rangle$ increases with $Re$, meaning that the suspension shows shear thickening behavior. We propose the scaling law can be described as $\langle \bar{\eta} \rangle = \langle \bar{\eta}_0 \rangle + kRe_p$, where $k$ is the slope of $\langle \bar{\eta} \rangle - Re_p$ curve depending on $Da$. The values of $k$ and coefficients of determination of the fits are given in Table 1. We can also verify that $\langle \bar{\eta}_0 \rangle$ is very close to the proposed scaling law for $\langle \bar{\eta}(Da) \rangle$ when neglecting the inertia of the particle and the fluids. From Table 1, we can also observe that the linear dependence decreases with the decreasing of Darcy number. For example, the determination coefficient of the linear fit is less than 0.99 when $Da = 10^{-5}$. Thus, it is more appropriate to approximate the $\langle \bar{\eta} \rangle - Re_p$ relation with the power-law relationship, as indicated in Fig. 11. At this sufficient small Darcy number, the inertial effect on the viscosity of porous particle suspensions agrees with that on the impermeable particle suspension, which is $\langle \bar{\eta} \rangle \propto Re_p^{1.5}$ as reported by Lin et al. [35], Mikulencak and Morris [36], and Subramanian and Koch [37].

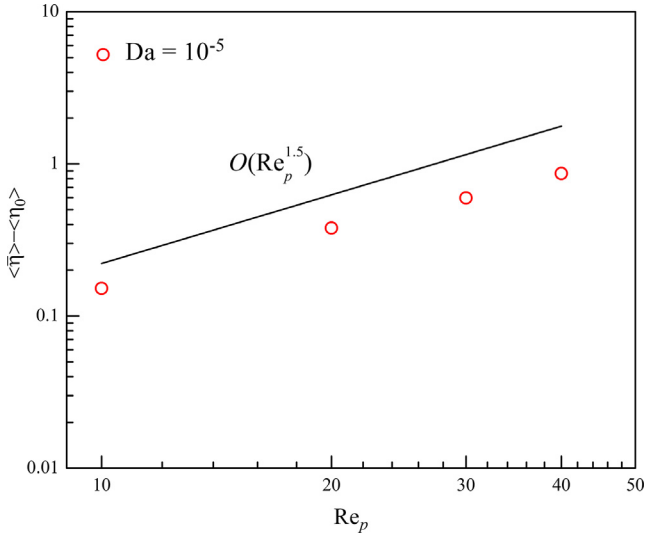


**Fig. 11.** Power-law dependence of the intrinsic viscosity as a function of Reynolds number for porous particle with $Da = 10^{-5}$.

## 4. Conclusions

In this work, we have presented three-dimensional lattice Boltzmann simulation of shear viscosity of dilute suspensions containing porous spherical particles. The fluid flow around and inside the porous particle is described by the volume-averaged macroscopic equations in terms of intrinsic phase average. The present method allows the analysis of Darcy number and the particle Reynolds number effect on the relative viscosity. The main findings are summarized as follows:

1. For a dilute suspension of porous spherical particles, the relative viscosity increases linearly with the particle volume fraction.
2. When neglecting the inertia of the suspension, its intrinsic viscosity only depends on the Darcy number: the intrinsic viscosity and $\log(Da)$ changes linearly at high $Da$ regime; while the dependence of intrinsic viscosity and $\log(Da)$ can be described by a second-degree polynomial at low $Da$ regime.
3. When the suspension is at the inertial flow regime, its intrinsic viscosity increases linearly with Reynolds number, and the increasing rate depends on Darcy number.

## Conflict of interest

The authors declare that there is no conflict of interests.

## Acknowledgement

This work was supported by the Research Grants Council of the Hong Kong Special Administrative Region, China (Grant 16209617).

## References

[1] S. Mueller, E.W. Llewellin, H.M. Mader, The rheology of suspensions of solid particles, Proc. Roy. Soc. A: Math. Phys. Eng. Sci. 466 (2116) (2010) 1201–1228, https://doi.org/10.1098/rspa.2009.0445.
[2] A. Einstein, Eine neue Bestimmung der Molekldimensionen, Ann. Phys. 324 (2) (1906) 289–306, https://doi.org/10.1002/andp.19063240204.
[3] G.K. Batchelor, J.T. Green, The determination of the bulk stress in a suspension of spherical particles to order $c^2$, J. Fluid Mech. 56 (3) (1972) 401–427, https://doi.org/10.1017/S0022112072002435.
[4] I.M. Krieger, T.J. Dougherty, A mechanism for non-Newtonian flow in suspensions of rigid spheres, Trans. Soc. Rheol. 3 (1) (1959) 137–152, https://doi.org/10.1122/1.548848.
[5] G.B. Jeffery, The motion of ellipsoidal particles immersed in a viscous fluid, Proc. Roy. Soc. A: Math. Phys. Eng. Sci. 102 (715) (1922) 161–179, https://doi.org/10.1098/rspa.1922.0078.
[6] D. Qi, L.-S. Luo, Rotational and orientational behaviour of three-dimensional spheroidal particles in Couette flows, J. Fluid Mech. 477 (2003) 201–213, https://doi.org/10.1017/S0022112002003191.
[7] S. Lishchuk, I. Halliday, C. Care, Shear viscosity of bulk suspensions at low reynolds number with the three-dimensional lattice Boltzmann method, Phys. Rev. E 74 (1) (2006) 017701, https://doi.org/10.1103/PhysRevE.74.017701.
[8] P.M. Kulkarni, J.F. Morris, Suspension properties at finite Reynolds number from simulated shear flow, Phys. Fluids 20 (4) (2008) 040602, https://doi.org/10.1063/1.2911017.
[9] H. Huang, X. Yang, M. Krafczyk, X.-Y. Lu, Rotation of spheroidal particles in Couette flows, J. Fluid Mech. 692 (2012) 369–394, https://doi.org/10.1017/jfm.2011.519.
[10] A. Xu, T. Zhao, L. Shi, X. Yan, Three-dimensional lattice Boltzmann simulation of suspensions containing both micro-and nanoparticles, Int. J. Heat Fluid Flow 62 (2016) 560–567, https://doi.org/10.1016/j.ijheatfluidflow.2016.08.001.
[11] H. Huang, Y. Wu, X. Lu, Shear viscosity of dilute suspensions of ellipsoidal particles with a lattice Boltzmann method, Phys. Rev. E 86 (4) (2012) 046305, https://doi.org/10.1103/PhysRevE.86.046305.
[12] M. Barrande, R. Bouchet, R. Denoyel, Tortuosity of porous particles, Anal. Chem. 79 (23) (2007) 9115–9121, https://doi.org/10.1021/ac071377r.
[13] E. Tasciotti, X. Liu, R. Bhavane, K. Plant, A.D. Leonard, B.K. Price, M.M.-C. Cheng, P. Decuzzi, J.M. Tour, F. Robertson, et al., Mesoporous silicon particles as a multistage delivery system for imaging and therapeutic applications, Nat. Nanotechnol. 3 (3) (2008) 151–157, https://doi.org/10.1038/nnano.2008.34.
[14] Z. Sun, X. Zhou, W. Luo, Q. Yue, Y. Zhang, X. Cheng, W. Li, B. Kong, Y. Deng, D. Zhao, Interfacial engineering of magnetic particles with porous shells: towards magnetic core-Porous shell microparticles, Nano Today 11 (4) (2016) 464–482, https://doi.org/10.1016/j.nantod.2016.07.003.
[15] H. Masoud, H.A. Stone, M.J. Shelley, On the rotation of porous ellipsoids in simple shear flows, J. Fluid Mech. 733. https://doi.org/10.1017/jfm.2013.476.
[16] C. Li, M. Ye, Z. Liu, On the rotation of a circular porous particle in 2D simple shear flow with fluid inertia, J. Fluid Mech. 808. https://doi.org/10.1017/jfm.2016.670.
[17] Z. Guo, T. Zhao, Lattice boltzmann model for incompressible flows through porous media, Phys. Rev. E 66 (3) (2002) 036304, https://doi.org/10.1103/PhysRevE.66.036304.
[18] L. Wang, L.-P. Wang, Z. Guo, J. Mi, Volume-averaged macroscopic equation for fluid flow in moving porous media, Int. J. Heat Mass Transf. 82 (2015) 357–368, https://doi.org/10.1016/j.ijheatmasstransfer.2014.11.056.
[19] H. Darcy, Les Fontaines Publiques de la Ville de Dijon: Exposition et Application, Victor Dalmont, 1856.
[20] H. Brinkman, A calculation of the viscous force exerted by a flowing fluid on a dense swarm of particles, Appl. Sci. Res. A1 (1947) 27–34, https://doi.org/10.1007/BF02120313.
[21] P. Debye, A. Bueche, Intrinsic viscosity, diffusion, and sedimentation rate of polymers in solution, J. Chem. Phys. 16 (6) (1948) 573–579, https://doi.org/10.1063/1.1746948.
[22] A. Xu, L. Shi, T. Zhao, Accelerated lattice Boltzmann simulation using GPU and OpenACC with data management, Int. J. Heat Mass Transf. 109 (2017) 577–588, https://doi.org/10.1016/j.ijheatmasstransfer.2017.02.032.
[23] P. Cheng, X. Quan, S. Gong, X. Liu, L. Yang, Chapter Four – Recent analytical and numerical studies on phase-change heat transfer, Adv. Heat Transf. 46 (2014) 187–248, https://doi.org/10.1016/bs.aiht.2014.08.004.
[24] Q. Li, K. Luo, Q. Kang, Y. He, Q. Chen, Q. Liu, Lattice Boltzmann methods for multiphase flow and phase-change heat transfer, Prog. Energy Combust. Sci. 52 (2016) 62–105, https://doi.org/10.1016/j.pecs.2015.10.001.
[25] R. Mei, D. Yu, W. Shyy, L.-S. Luo, Force evaluation in the lattice Boltzmann method involving curved geometry, Phys. Rev. E 65 (4) (2002) 041203, https://doi.org/10.1103/PhysRevE.65.041203.
[26] B. Wen, C. Zhang, H. Fang, Hydrodynamic force evaluation by momentum exchange method in lattice Boltzmann simulations, Entropy 17 (12) (2015) 8240–8266, https://doi.org/10.3390/e17127876.
[27] B. Wen, C. Zhang, Y. Tu, C. Wang, H. Fang, Galilean invariant fluid-solid interfacial dynamics in lattice Boltzmann simulations, J. Comput. Phys. 266 (2014) 161–170, https://doi.org/10.1016/j.jcp.2014.02.018.
[28] A. Xu, W. Shyy, T. Zhao, Lattice Boltzmann modeling of transport phenomena in fuel cells and flow batteries, Acta. Mech. Sin. 33 (3) (2017) 555–574, https://doi.org/10.1007/s10409-017-0667-6.
[29] A.J. Ladd, Numerical simulations of particulate suspensions via a discretized Boltzmann equation. Part 1. Theoretical foundation, J. Fluid Mech. 271 (1994) 285–309, https://doi.org/10.1017/S0022112094001771.
[30] A.J. Ladd, Numerical simulations of particulate suspensions via a discretized Boltzmann equation. Part 2. Numerical results, J. Fluid Mech. 271 (1994) 311–339, https://doi.org/10.1017/S0022112094001783.
[31] B. Felderhof, Frictional properties of dilute polymer solutions: III. Translational-friction coefficient, Phys. A: Stat. Mech. Appl. 80 (1) (1975) 63–75, https://doi.org/10.1016/0378-4371(75)90146-6.
[32] H. Huang, X.-Y. Lu, An ellipsoidal particle in tube Poiseuille flow, J. Fluid Mech. 822 (2017) 664–688, https://doi.org/10.1017/jfm.2017.298.
[33] A.J. Wagner, I. Pagonabarraga, Lees-Edwards boundary conditions for lattice Boltzmann, J. Stat. Phys. 107 (1) (2002) 521–537, https://doi.org/10.1023/A:1014595628808.
[34] E. Lorenz, A.G. Hoekstra, A. Caiazzo, Lees-Edwards boundary conditions for lattice Boltzmann suspension simulations, Phys. Rev. E 79 (3) (2009) 036706, https://doi.org/10.1103/PhysRevE.79.036706.
[35] C.-J. Lin, J.H. Peery, W. Schowalter, Simple shear flow round a rigid sphere: inertial effects and suspension rheology, J. Fluid Mech. 44 (1) (1970) 1–17, https://doi.org/10.1017/S0022112070001659.
[36] D.R. Mikulencak, J.F. Morris, Stationary shear flow around fixed and free bodies at finite reynolds number, J. Fluid Mech. 520 (2004) 215–242, https://doi.org/10.1017/S0022112004001648.
[37] G. Subramanian, D.L. Koch, Inertial effects on the transfer of heat or mass from neutrally buoyant spheres in a steady linear velocity field, Phys. Fluids 18 (7) (2006) 073302, https://doi.org/10.1063/1.2215370.